J Braz. Soc. Mech. Sci. Eng. manuscript No.
(will be inserted by the editor)

Non-intrusive polynomial chaos expansion for topology optimization using polygonal meshes

Nilton Cuellar · Anderson Pereira · Ivan F. M. Menezes · Americo Cunha Jr

Received: date / Accepted: date

arXiv:2108.01616v1 [cs.CE] 14 Jul 2021

Abstract This paper deals with the applications of stochastic spectral methods for structural topology optimization in the presence of uncertainties. A non-intrusive polynomial chaos expansion is integrated into a topology optimization algorithm to calculate low-order statistical moments of the mechanical-mathematical model response. This procedure, known as robust topology optimization, can optimize the mean of the compliance while simultaneously minimizing its standard deviation. In order to address possible variabilities in the loads applied to the mechanical system of interest, magnitude and direction of the external forces are assumed to be uncertain. In this probabilistic framework, forces are described as a random field or a set of random variables. Representation of the random objects and propagation of load uncertainties through the model are efficiently done through Karhunen–Loève and polynomial chaos expansions. We take advantage of using polygonal elements, which have been shown to be effective in suppressing checkerboard patterns and reducing mesh dependency in the solution of topology optimization problems. Accuracy and applicability of the proposed methodology are demonstrated by means of several topology optimization examples. The obtained results, which are in excellent agreement with reference solutions computed via Monte Carlo method, show that load uncertainties play an important role in optimal design of structural systems, so that they must be taken into account to ensure a reliable optimization process.

N. Cuellar · A. Pereira · I. F. M. Menezes
Pontifical Catholic University of Rio de Janeiro – PUC–Rio, Department of Mechanical Engineering, Rua Marquês de São Vicente, 225, Rio de Janeiro, 22453-900, RJ, Brazil
E-mail: ncuellar@tecgraf.puc-rio.br
E-mail: anderson@tecgraf.puc-rio.br
E-mail: ivan@puc-rio.br

A. Cunha Jr
Universidade do Estado do Rio de Janeiro – UERJ, Nucleus of Modeling and Experimentation with Computers – NUMERICO, Rua São Francisco Xavier, 524, Rio de Janeiro, 20550-900, RJ, Brazil
E-mail: americo@ime.uerj.br

Keywords topology optimization · stochastic spectral approach · polynomial chaos · Karhunen–Loève expansion · robust optimization · polygonal finite element

1 Introduction

Due to new requirements of design associated with the most modern engineering applications, mechanical systems with very complex geometrical configurations are becoming increasingly common. In this context, some of the most promising design approaches are based on topology optimization (TO), which seeks to find the best layout for a system, by optimizing the material distribution in a predefined design domain [35, 8]. The growing popularity of TO solutions is demonstrated by their wide range of application in various fields such as structural mechanics [58, 59, 45, 43, 17, 33], composite and multi-materials [62, 67], nanotecnology [36], fluid mechanics [39, 19], fluid-structure interaction [1], medicine [38], etc.

In general, the physical systems underlying TO applications are subjected to a series of uncertainties (e.g. unknown loads, geometrical imperfections, fluctuations in physical properties, etc) so that, usually, their response is not well predicted by the traditional (deterministic) tools of engineering analysis. For this reason, there is a consensus among computational engineering experts that uncertainties effects must be incorporated into any computational predictive model [49]. The modeling and quantification of uncertainties is necessary in order to predict a possible range of variability for the mathematical model response, and to conduct applied tasks, such as analysis and design, in a robust way [5, 51]. Notice, however, that the majority of the works in TO area, currently available in the literature, are limited to deterministic analyses.

The need for robust design and analysis of uncertainties in topological optimization applications naturally induces the search for computationally efficient frameworks for TO. For this purpose, TO literature started to take uncertainty quantification (UQ) into account over the last decade, as can be seen in several papers addressing the two issues [65, 28, 16, 66, 42, 44, 68, 20, 27, 60, 3, 14, 25, 29, 61].

Some of these works are based on classical techniques for stochastic computation like Monte Carlo (MC) method [14, 20] or series expansion [16, 68, 27, 3, 25] which, despite of being very simple in conceptual terms, they are limited by the high computational cost, the former, or very small range of applicability, the latter. These limitations open space for spectral-based approaches [29, 60, 44, 65, 42, 28], that use state-of-the-art tools for representing and propagating uncertainties in computational models, like Karhunen–Loève (KL) and generalized polynomial chaos (gPC) expansions. A recent work by Keshavarzzadeh et. al [28] presents a non-intrusive gPC strategy to propagate uncertainties in topology optimization problems. They use non-intrusive polynomial chaos expansion to evaluate low-order statistics of compliance and volume and the uncertainties are considered in the applied loads and also in the geometry of the problems.

The classical formulation for topology optimization, which corresponds to minimize the structural compliance, is commonly carried out on uniform grids consisting of Lagrangian-type finite elements (e.g., linear quads). However, this choice of discretization, together with density methods, suffer from the well-known numerical instabilities, such as the checkerboard patterns. Unstructured "Voronoi"

meshes, generated from an initial set of random points, have been shown to be effective in suppressing checkerboard patterns [58]. Moreover, compared to standard Lagrangian-type uniform grids, polygonal elements are more versatile in discretizing complex domains and in reducing mesh dependency in the solutions of topology optimization [58, 2]. The geometrical flexibility of the polygonal finite elements also make them very attractive for adaptive mesh refinement schemes in topology optimization problems [37, 26]. The computational code used here was developed based on PolyTop [59], a MATLAB code for solving topology optimization problems using either structured or unstructured polygonal meshes in arbitrary two-dimensional domains. The modular structure of `PolyTop`, where the analysis routine and optimization algorithm are separated from the choice of topology optimization formulation, together with a non-intrusive way of computing the statistical measures, allowed us to implement a robust topology optimization code in a very straightforward way, with only a few modifications in the original `PolyTop` code.

The aim of this paper is to present a computationally efficient and accurate non-intrusive robust topology optimization approach using polygonal elements. For this purpose, the `PolyTop` framework by Talischi et al. [59], which employs polygonal finite elements in TO, is combined with a consistent methodology for stochastic analysis that uses a non-intrusive gPC strategy to propagate parameters uncertainties through the computational model. This combination generates a framework that is computationally efficient for stochastic simulations, and robust to numerical instabilities typical of TO problems, such as checkerboards, one-node connections, and mesh dependency. The novel approach is used to solve TO problems that seek to minimize an objective function based on the low-order statistical moments of the compliance function of a structure, subjected to uncertainties on the external load, and satisfying volume constraints.

The remainder of this paper is organized as follows. Stochastic spectral methods are introduced in section 2, together with the mathematical formulation and basic steps to obtain KL and gPC expansions. In section 3, the TO problem is briefly described, as well as stochastic procedure to propagate uncertainties within TO, which is called robust topology optimization (RTO). In section 4, numerical examples are presented, and the proposed methodology is compared with a reference result obtained with MC method. Finally, some remarks and suggestions for future work are presented in section 5.

2 Stochastic spectral methods

2.1 Preliminary definitions and notation

Consider a probability space $(\Theta, \mathcal{F}, P)$, where Θ is the sample space, $\mathcal{F}$ a σ-field over Θ, and $P : \mathcal{F} \to [0, 1]$ denotes the probability measure. It is assumed that the distribution $P_X(dx)$ of any real-valued random variable X in this probability space admits a density $x \mapsto p_X(x)$ with respect to dx. The set of values where this density is not zero is dubbed the support of X, being denoted by $\mathtt{Supp}\, X$.

In this probabilistic setting, any realization of random variable X is denoted by $X(\theta)$ for $\theta \in \Theta$, and the mathematical expectation operator is defined by

$$E\{X\} = \int_{\mathbb{R}} x \; P_X(dx), \tag{1}$$

so that the mean value and standard deviation of X are given by $\mu_X = E\{X\}$ and $\sigma_X = (E\left\{X^2\right\} - E\{X\}^2)^{1/2}$, respectively. The random variable X is said to be of second-order if

$$E\left\{|X|^2\right\} = \int_{\mathbb{R}} |x|^2 \; P_X(dx) \; < \; +\infty. \tag{2}$$

The space of all second-order random variables in $(\Theta, \mathcal{F}, P)$, denoted by $L_2(\Theta, P)$, is a Hilbert space [12] equipped with the inner product $\langle \cdot, \cdot \rangle_\Theta : L_2(\Theta, P) \times L_2(\Theta, P) \to \mathbb{R}$ such that

$$\langle X, Y \rangle_\Theta = E\{X\,Y\} = \int \int_{\mathbb{R}^2} x\, y \; P_{X,Y}(dx, dy), \tag{3}$$

where $P_{X,Y}(dx, dy)$ is the joint distribution of the random variables $X, Y \in L_2(\Theta, P)$. This inner product induces a norm $\|\cdot\|_\Theta : L_2(\Theta, P) \to \mathbb{R}$ where

$$\|X\|_\Theta = \left(\langle X, X \rangle_\Theta\right)^{1/2} = \left(\int_{\mathbb{R}} |x|^2 \; P_X(dx)\right)^{1/2}. \tag{4}$$

Further ahead it will also be helpful to consider $L_2(\mathcal{D})$, the set of all real-valued square integrable functions defined on the spatial domain $\mathcal{D} \subset \mathbb{R}^d$, $d \geq 1$. This set of functions is also a Hilbert space [12], with inner product $\langle \cdot, \cdot \rangle_\mathcal{D} : L_2(\mathcal{D}) \times L_2(\mathcal{D}) \to \mathbb{R}$ defined by

$$\left\langle \phi, \phi' \right\rangle_\mathcal{D} = \int_\mathcal{D} \phi(\mathbf{x})\, \phi'(\mathbf{x})\, d\mathbf{x}, \tag{5}$$

for $\phi, \phi' \in L_2(\mathcal{D})$.

2.2 Karhunen–Loève expansion

The KL expansion [24, 63] is one of the most widely used and powerful techniques for analysis and synthesis of random fields, providing a denumerable representation, in terms of the spectral decomposition of the correlation function, for a random field parametrized by a nondenumerable index [51, 53].

Let the map $(\mathbf{x}, \theta) \in \mathcal{D} \times \Theta \mapsto U(\mathbf{x}, \theta) \in \mathbb{R}$ be an arbitrary real-valued random field, indexed by the spatial coordinate vector $\mathbf{x} \in \mathcal{D} \subset \mathbb{R}^d$, $d \geq 1$, denoted in an abbreviated way as $U(\mathbf{x})$ or U. By construction, for a fixed $\mathbf{x} \in \mathcal{D}$, $U(\mathbf{x}, \cdot)$ is a real-valued random variable, and $U(\cdot, \theta)$, for a fixed $\theta \in \Theta$, is a function of $\mathbf{x}$, dubbed realization of the random field.

The correlation of $U(\mathbf{x})$ is the function $\mathcal{K}_U(\cdot, \cdot) : \mathcal{D} \times \mathcal{D} \to \mathbb{R}$ defined for any pair of vectors $\mathbf{x}$ and $\mathbf{x}'$ by means of

$$\mathcal{K}_U(\mathbf{x}, \mathbf{x}') = E\left\{U(\mathbf{x})\, U(\mathbf{x}')\right\}. \tag{6}$$

Suppose that random field $U(\mathbf{x})$ is second-ordered and mean-square continuous, properties respectively defined by

$$E\left\{|U(\mathbf{x})|^2\right\} < +\infty, \quad \forall\, \mathbf{x} \in \mathcal{D}, \tag{7}$$

and

$$\lim_{\mathbf{x}' \to \mathbf{x}} \left\| U(\mathbf{x}') - U(\mathbf{x}) \right\|_{\Theta}^2 = 0. \tag{8}$$

Under these assumptions, the linear integral operator

$$\mathcal{K}_U\, \phi\,(\mathbf{x}) = \int_{\mathcal{D}} \mathcal{K}_U(\mathbf{x}, \mathbf{x}')\, \phi(\mathbf{x}')\, d\mathbf{x}' \tag{9}$$

defines a Hilbert-Schmidt operator [53, 51], which has denumerable family of eigenpairs $\left\{(\lambda_n, \phi_n)\right\}_{n=1}^{+\infty}$ such that

$$\int_{\mathcal{D}} \mathcal{K}_U(\mathbf{x}, \mathbf{x}')\, \phi_n(\mathbf{x}')\, d\mathbf{x}' = \lambda_n\, \phi_n(\mathbf{x}), \qquad \mathbf{x} \in \mathcal{D}, \tag{10}$$

where λ_n are the eigenvalues and ϕ_n the corresponding eigenfunctions of the operator defined by Eq.(9). Besides that, the sequence of eigenvalues is such that $\sum_{n=1}^{+\infty} \lambda_n < +\infty$ and $\lambda_1 \geq \lambda_2 \geq \cdots \geq \lambda_n \geq \cdots \to 0$; and the family of functions $\{\phi_n\}_{n=1}^{+\infty}$ defines an orthonormal Hilbertian basis in $L_2(\mathcal{D})$, i.e.

$$\langle \phi_m, \phi_n \rangle_{\mathcal{D}} = \delta_{mn}\,, \tag{11}$$

where Kronecker delta is such that $\delta_{mn} = 1$ if $m = n$ and $\delta_{mn} = 0$ for $m \neq n$.

Therefore, applying two standard results of functional analysis [15], the theorems of Hilbertian basis and orthogonal projection, it is possible to show that the random field $U(\mathbf{x})$ admits a decomposition

$$U(\mathbf{x}) = \mu_{\,U}(\mathbf{x}) + \sum_{n=1}^{+\infty} \sqrt{\lambda_n}\, \phi_n(\mathbf{x})\, \xi_n\,, \tag{12}$$

where $\{\xi_n\}_{n=1}^{+\infty}$ is a family of random variables defined by

$$\xi_n = \frac{1}{\sqrt{\lambda_n}}\, \langle U - \mu_{\,U}, \phi_n \rangle_{\mathcal{D}}\,, \tag{13}$$

which are centered (zero mean) and mutually uncorrelated i.e.

$$\mu_{\xi_n} = 0, \qquad \text{and} \qquad E\left\{\xi_m\, \xi_n\right\} = \delta_{mn}\,. \tag{14}$$

A finite dimensional approximation for $U(\mathbf{x})$, denoted by $U^{\nu_{kl}}(\mathbf{x})$, is constructed by truncation of the series in Eq.(12) i.e.

$$U^{\nu_{kl}}(\mathbf{x}) = \mu_{\,U}(\mathbf{x}) + \sum_{n=1}^{\nu_{kl}} \sqrt{\lambda_n}\, \phi_n(\mathbf{x})\, \xi_n, \tag{15}$$

where the integer ν_{kl} is chosen such that

$$\texttt{energy}(\nu_{kl}) = \frac{\sum_{n=1}^{\nu_{kl}} \lambda_n}{\sum_{n=1}^{+\infty} \lambda_n} \geq \tau, \tag{16}$$

for a heuristically chosen threshold τ (e.g. $\tau = 90\%$). In practice, as a closed formula for λ_n is not available in general, $\texttt{energy}(\nu_{kl})$ is estimated using a finite (but large) number of eigenvalues, instead of an infinite quantity. This procedure is justified in light of the eigenvalues decreasing property.

One of the main difficulties to apply KL expansion to discrete random fields is the determination of the eigenvalues and corresponding eigenfunctions of the correlation function. Analytical solutions for the Fredholm integral equation in (10) are almost never available. However, for some special cases, such as exponential and Gaussian autocovariance functions, an analytical solution can be obtained by converting the integral equation into a differential equation through successive derivatives [24, 63].

Several numerical methods can be used to solve the eigenvalue problem of Eq.(10), such as the direct method, projection methods, among others [4, 9]. In this study, the direct method is employed to transform the Fredholm integral equation into a finite dimensional eigenvalue problem, whose the solution provides an approximation for the desired eigenvalues/eigenvectors of the infinite dimensional problem.

In this numerical procedure, a set of M realizations of the random field $U(\mathbf{x})$ and its mean function $\mu_U(\mathbf{x})$ are numerically generated[1] and grouped into the matrices

$$\boldsymbol{U} = \begin{bmatrix} U^1(\mathbf{x}_1) & U^2(\mathbf{x}_1) & \dots & U^M(\mathbf{x}_1) \\ U^1(\mathbf{x}_2) & U^2(\mathbf{x}_2) & \dots & U^M(\mathbf{x}_2) \\ \vdots & \vdots & \ddots & \vdots \\ U^1(\mathbf{x}_n) & U^2(\mathbf{x}_n) & \dots & U^M(\mathbf{x}_n) \end{bmatrix}, \boldsymbol{\mu} = \begin{bmatrix} \mu_U(\mathbf{x}_1) & \mu_U(\mathbf{x}_1) & \dots & \mu_U(\mathbf{x}_1) \\ \mu_U(\mathbf{x}_2) & \mu_U(\mathbf{x}_2) & \dots & \mu_U(\mathbf{x}_2) \\ \vdots & \vdots & \ddots & \vdots \\ \mu_U(\mathbf{x}_n) & \mu_U(\mathbf{x}_n) & \dots & \mu_U(\mathbf{x}_n) \end{bmatrix}, \quad (17)$$

which are used to define the zero mean matrix $\hat{\boldsymbol{U}} = \boldsymbol{U} - \boldsymbol{\mu}$. Then, the correlation matrix is estimated with the aid of

$$\mathcal{K}_{\hat{\boldsymbol{U}}} = \frac{1}{M}\hat{\boldsymbol{U}}\hat{\boldsymbol{U}}^T, \quad (18)$$

and the discrete eigenvalue problem

$$\mathcal{K}_{\hat{\boldsymbol{U}}}\boldsymbol{\Phi} = \boldsymbol{\Lambda}\boldsymbol{\Phi}, \quad (19)$$

is solved to obtain the matrices $\boldsymbol{\Phi}$ and $\boldsymbol{\Lambda}$, which present approximations for the first M eigenfunctions/eigenvalues on the columns/main diagonal.

For further details on theoretical and practical aspects of KL expansion the reader is encouraged to see [34, 6, 40, 41].

2.3 Generalized polynomial chaos expansion

The gPC expansion is a theoretical tool used to construct representations for random fields, with a denumerable or nondenumerable set of index, in terms of a denumerable collection of random variables weigthed by deterministic coefficients [51, 53]. It was introduced in the engineering community by R. Ghanem [24, 55, 22]

[1] These numerical realizations are defined in a computational mesh $\mathbf{x}_1, \mathbf{x}_2, \cdots, \mathbf{x}_n$.

as a tool to compute approximate responses for problems involving random fields with unknown distribution and since the early 2000s, especially after the work of Xiu and Karniadakis [64], it has been used in many applications of computational stochastic mechanics, a trend that should increase [56].

For the sake of theoretical development, consider a second-ordered random variable $U : \Theta \to \mathbb{R}$ which can be written in terms of a (possibly infinity) set of independent random variables $\xi_1(\theta), \xi_2(\theta), \xi_3(\theta), \cdots$. Collecting these independent variables into the random vector $\boldsymbol{\xi}(\theta) = (\xi_1(\theta), \xi_2(\theta), \xi_3(\theta), \cdots)$, dubbed the germ, it is possible to rewrite the original variable in the parametric form $U = U(\boldsymbol{\xi})$.

In this context of second-ordered random variables, gPC expansion theory says that such random variable U admits a spectral representation

$$U(\boldsymbol{\xi}) = \sum_{n=0}^{+\infty} u_n \, \psi_n(\boldsymbol{\xi}), \tag{20}$$

where the set of orthonormal polynomials $\{\psi_0, \psi_1, \psi_2, \cdots\}$ is a basis for $L_2(\Theta, P)$, and the deterministic coefficients $u_0, u_1, u_2, \cdots$ correspond to the coordinates of U in this infinite dimensional base. By definition $\psi_0(\boldsymbol{\xi}) = 1$, and due to the orthogonality property $\langle \psi_m, \psi_n \rangle_\Theta = \delta_{mn}$, one has

$$\begin{aligned} \mu_U &= E\{U\} \\ &= E\{\psi_0 \, U\} \\ &= \sum_{n=0}^{+\infty} u_n \, \langle \psi_0, \psi_n \rangle_\Theta \\ &= u_0, \end{aligned} \tag{21}$$

i.e., the mean of U is equal to the coordinate u_0 of gPC expansion. Besides that, it is easy to see that $E\{\psi_n\} = 0, \ n \geq 1$. Thus, it can also be shown that standard deviation of U can be written as

$$\begin{aligned} \sigma_U^2 &= E\left\{U^2\right\} - E\{U\}^2 \\ &= E\left\{ \left(\sum_{n=1}^{+\infty} u_n \, \psi_n(\boldsymbol{\xi}) \right)^2 \right\} \\ &= \sum_{n=1}^{+\infty} u_n^2. \end{aligned} \tag{22}$$

The gPC expansion has attracted the attention of many researchers due to its rapid convergence property and its capability to estimate statistical moments, which allows this method to efficiently reduce computational effort in highly nonlinear engineering design applications [34, 41].

Of course, for any purpose of numerical computation, it is necessary to parametrize the random variable U with a finite number ν_{rv} of independent random variables, i.e., $\boldsymbol{\xi} = (\xi_1, \xi_2, \cdots, \xi_{\nu_{rv}})$, and restrict up to p_{pc} the order of the polynomials in the basis, so that the series in Eq.(20) is truncated with $\nu_{pc}+1 = (\nu_{rv}+p_{pc})!/(\nu_{rv}!\, p_{pc}!)$ terms, giving rise to the approximation

$$U^{\nu_{pc}}(\boldsymbol{\xi}) = \sum_{n=0}^{\nu_{pc}} u_n \, \psi_n(\boldsymbol{\xi}), \tag{23}$$

which is mean-square convergent to U when $p_{pc}, \nu_{rv} \to +\infty$.

In practice, ν_{rv} is obtained from the stochastic modeling and p_{pc} is specified such that a compromise between accuracy and efficiency can be established. In this work, the gPC polynomial order is selected such that the low-order statistics estimations become invariant for increasing values of p_{pc}.

This spectral expansion can be easily extended to a second-ordered random field $U : \mathcal{D} \times \Theta \to \mathbb{R}$, considering this field as a family of random variables $U(\mathbf{x}, \cdot) \in L_2(\Theta, P)$, parameterized by the index $\mathbf{x}$, and by letting the deterministic coefficients of the gPC expansion depend on $\mathbf{x}$, i.e.

$$U(\mathbf{x}, \boldsymbol{\xi}) = \sum_{n=0}^{+\infty} u_n(\mathbf{x})\, \psi_n(\boldsymbol{\xi}), \tag{24}$$

where the coordinates are now a deterministic function of $\mathbf{x}$. As in the case of a random variable, the truncation of the series in Eq.(24) results in the approximation

$$U^{\nu_{pc}}(\mathbf{x}, \boldsymbol{\xi}) = \sum_{n=0}^{\nu_{pc}} u_n(\mathbf{x})\, \psi_n(\boldsymbol{\xi}). \tag{25}$$

Basically, two approaches for implementing the gPC expansion are available in the literature, one called the intrusive, and another one dubbed non-intrusive. The intrusive approach is based on a stochastic version of Galerkin method [63], and consists in modifying the deterministic model in order to take into account the uncertainty propagation. The main disadvantage of this formalism is related to the level of difficulty in modifying the code associated with the deterministic model, particularly if commercial software is being used, due to code access restrictions [51, 23].

On the other hand, the non-intrusive approach requires no modification in the deterministic model and therefore, can be treated as a black box [51, 23]. In this case, a probabilistic collocation approach, based on a sparse grid method [21], can be used to estimate the coefficients (coordinates) of the expansion. In this work, a different non-intrusive approach based on linear regression is employed, where the random field (variable) of interest is evaluated in a finite set of ν_{gq} possible realizations of the germ $\boldsymbol{\xi}$, and thus the coefficients of the expansion are obtained through $\mathbf{u} = (\boldsymbol{\Psi}^T \boldsymbol{\Psi})^{-1} \boldsymbol{\Psi}^T \mathbf{U}$, the solution of the mean-square problem

$$\boldsymbol{\Psi}\, \mathbf{u} \;\approx\; \mathbf{U}, \tag{26}$$

where

$$\underbrace{\begin{bmatrix} \psi_0(\boldsymbol{\xi}_1) & \cdots & \psi_{\nu_{pc}}(\boldsymbol{\xi}_1) \\ \vdots & \ddots & \vdots \\ \psi_0(\boldsymbol{\xi}_{\nu_{gq}}) & \cdots & \psi_{\nu_{pc}}(\boldsymbol{\xi}_{\nu_{gq}}) \end{bmatrix}}_{\boldsymbol{\Psi}} \underbrace{\begin{bmatrix} u_0 \\ u_1 \\ \vdots \\ u_{\nu_{pc}} \end{bmatrix}}_{\boldsymbol{u}} \approx \underbrace{\begin{bmatrix} U(\mathbf{x}, \boldsymbol{\xi}_1) \\ \vdots \\ U(\mathbf{x}, \boldsymbol{\xi}_{\nu_{gq}}) \end{bmatrix}}_{\boldsymbol{U}}. \tag{27}$$

For further information about the basic aspects of gPC expansion the reader is encouraged to see the references [24, 63, 34, 41, 23, 31], and for more advanced topics [53, 52, 50, 54, 32].

3 Topology optimization

3.1 Classical topology optimization

The main objective of TO is to find the optimal distribution of materials, for every point $\mathbf{x}$ in a given design domain $\Omega \subset \mathbb{R}^d$, $d = 2$ or 3, which maximize a certain performance measure subjected to a set of design constraints, i.e., to determine which regions in Ω should not present material (void regions), and obtain the final topology of the structure.

By convention, points where material exists are represented by a density value of 1, otherwise, the density value is 0. Note that, in this way, one has an integer-programming problem, where the distribution of material is defined by the density map $\mathbf{x} \in \Omega \mapsto \rho(\mathbf{x}) \in \{0, 1\}$, for

$$\rho(\mathbf{x}) = \begin{cases} 1 & \text{if } \mathbf{x} \text{ is structural member,} \\ 0 & \text{if } \mathbf{x} \text{ is void.} \end{cases} \tag{28}$$

In this paper the optimization problem seeks to minimize an objective function defined by the continuum structure compliance, denoted here by c, subject to a constraint on the final volume of the structure and satisfying the equilibrium equations for a linear Hookean solid material. This formulation, which is equivalent to maximize the structural stiffness subject to the same constraints (see reference [8] for further details), can be stated as

$$\begin{aligned} \min_{\rho} \quad & c\left(\mathbf{u}(\rho), \rho\right) = \int_{\Omega} \frac{1}{2}\, \boldsymbol{\sigma} : \boldsymbol{\epsilon}\; d\Omega, \\ s.t. \quad & v(\rho) = \int_{\Omega} \rho(\mathbf{x})\, d\Omega \leq v_S, \end{aligned} \tag{29}$$

where $\boldsymbol{\sigma}$ and $\boldsymbol{\epsilon}$ represent the tensors of stress and strain, respectively, v_S is a specified upper bound on the optimized structure volume, and the map $\mathbf{x} \in \Omega \mapsto \mathbf{u}(\rho(\mathbf{x})) \in \mathbb{R}^d$ is the continum structure displacement, parametrized by ρ and implicitly defined by the elasticity equations

$$\begin{aligned} \nabla \cdot \boldsymbol{\sigma}(\mathbf{u}) &= \mathbf{0}, \\ \boldsymbol{\sigma}(\mathbf{u}) &= \boldsymbol{\sigma}(\mathbf{u})^T, \\ \boldsymbol{\epsilon}(\mathbf{u}) &= \tfrac{1}{2}\left(\nabla \mathbf{u} + \nabla \mathbf{u}^T\right), \\ \boldsymbol{\sigma}(\mathbf{u}) &= \boldsymbol{\mathcal{C}}(\rho) : \boldsymbol{\epsilon}(\mathbf{u}), \end{aligned} \tag{30}$$

and the boundary conditions

$$\begin{aligned} \boldsymbol{\sigma}(\mathbf{u}) \cdot \mathbf{n} &= \boldsymbol{t} \;\text{ in } \Gamma_N, \\ \mathbf{u} &= \mathbf{0} \;\text{ in } \Gamma_D, \end{aligned} \tag{31}$$

where Γ_D is the partition of $\partial\Omega$ on which the displacements are prescribed, Γ_N is the complimentary partition of $\partial\Omega$ on which tractions $\mathbf{t}$ are prescribed such that $\overline{\Gamma_D} \cup \overline{\Gamma_N} = \partial\Omega$ and $\Gamma_D \cap \Gamma_N = \emptyset$ and $\boldsymbol{\mathcal{C}}(\rho)$ is the $4th$ order stiffness tensor that depends on the density function ρ. As posed, finding ρ and $\boldsymbol{\mathcal{C}}(\rho)$ becomes a large integer programming problem, which can be impractical to solve. Thus, we recast ρ as a continuous scalar field, $\rho(\mathbf{x}) \in [0, 1]$. In order to recover the binary nature

of the problem, the SIMP [8] model is employed and the stiffness tensor can be expressed as

$$\boldsymbol{\mathcal{C}}(\rho) = \left[\varepsilon + (1-\varepsilon)\rho^p\right] \boldsymbol{\mathcal{C}}^0, \tag{32}$$

where $p > 1$ is the penalty parameter, $\boldsymbol{\mathcal{C}}^0$ is the elasticity tensor of the constituent material, and $0 < \varepsilon \ll 1$ is a positive parameter ensuring well-posedness of the governing equations.

In terms of computational implementation, the domain is splited into N elementary regions, i.e., $\Omega = \cup_{e=1}^{N} \Omega^e$, and the finite element method is employed for the solution of the elasticity equations. Thus, the following finite dimensional version of the optimization problem is considered

$$\min_{\boldsymbol{\rho}} \; C(\boldsymbol{\rho}) = \mathbf{F}^{\,T}\, \mathbf{U}(\boldsymbol{\rho}), \tag{33}$$

$$\text{s.t.} \; V(\boldsymbol{\rho}) = \sum_{e=1}^{N} \rho_e \, |\Omega^e| - v_S \leq 0, \tag{34}$$

$$\text{with} \; \boldsymbol{K}(\boldsymbol{\rho})\, \mathbf{U}(\boldsymbol{\rho}) = \mathbf{F}, \tag{35}$$

where $\boldsymbol{\rho} = (\rho_1, \rho_2, \cdots, \rho_N)$ is a discretized version of the density map, $|\Omega^e|$ denotes the volume of the element e, $\mathbf{U}$ is the discrete displacement vector, parametrized by $\boldsymbol{\rho}$ and implicitly defined by the equilibrium equation, $\mathbf{F}$ is the global loading vector and $\boldsymbol{K}$ represents the global stiffness matrix, which is also dependent on $\boldsymbol{\rho}$.

In order to use gradient-based optimization algorithms to solve the above formulation, gradients of the objective function as well as the volume constraint function are needed. The sensitivity of the objective function $C(\boldsymbol{\rho})$ with respect to the design variables $\boldsymbol{\rho}$, is expressed in component form as

$$\frac{\partial C}{\partial \rho_e} = -\mathbf{U}^T \frac{\partial \boldsymbol{K}}{\partial \rho_e} \mathbf{U}. \tag{36}$$

The gradient of the volume constraint function $V(\boldsymbol{\rho})$ with respect to the design variable ρ_e is given as

$$\frac{\partial V}{\partial \rho_e} = |\Omega^e|. \tag{37}$$

During the solution of a TO problem it is very common to deal with numerical anomalies, such as checkerboards, which are traditionally treated through the use of higher-order elements or filters [48, 13]. However, Talischi et al. [59] have shown that the use of the `PolyTop` framework, which employs polygonal finite elements, can naturally address the checkerboard problem. Besides that, this approach also allows flexibility in the optimization strategy to be used, being compatible with the classical approaches based on the optimality criteria (OC) [7] and the method of moving asymptotes (MMA) [57].

An overview of the classical TO procedure, used in `PolyTop` framework to obtain an optimal design, is illustrated in Figure 1. The sensitivity analysis step described in this schematic is explained in details in section 3.5.

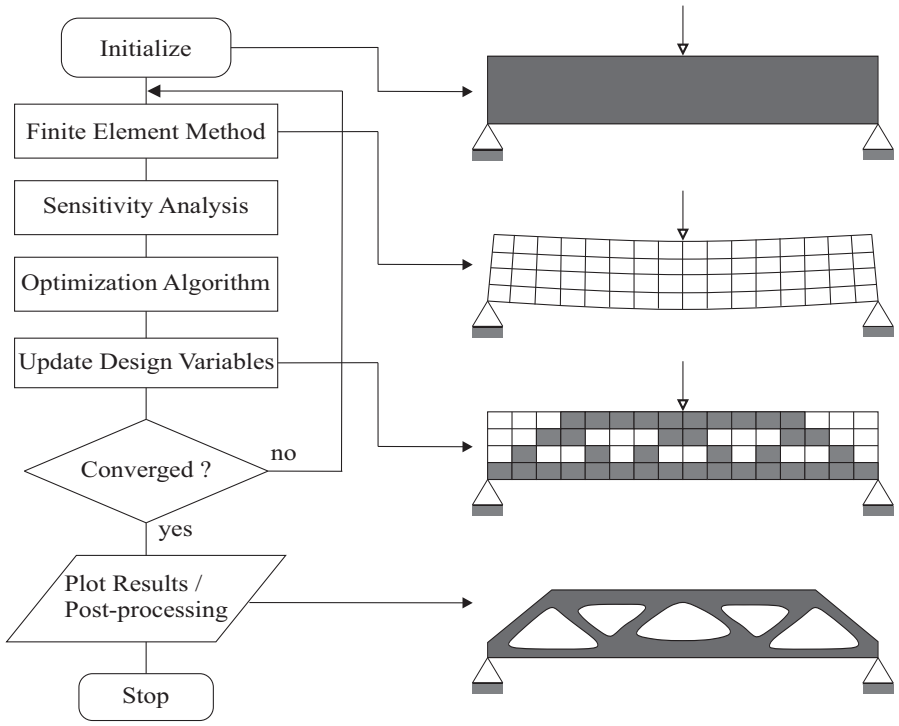


Figure 1 Overview of the classical topology optimization procedure (adapted from [8]).

3.2 Robust design optimization

Robust optimization, also known as robust design optimization (RDO), is a mathematical procedure that simultaneously addresses optimization and robustness analysis, obtaining an optimal design that is less susceptible to variabilities (uncertainties) in the system parameters. In contrast to conventional optimization, that is deterministic, RDO considers parameters that are random so that it consists of a stochastic problem. The general overview of RDO is explained in Figure 2, which shows a computational model where the input is subjected to uncertainties — that can be in material or geometrical properties, loadings, boundary conditions etc. — and, therefore, the model response has a certain probability distribution. This distribution is used to compute some kind of statistical response of the system, which is conveniently used to update the model input, in order to reduce the output uncertainty.

In this context, it is essential to understand the mathematical definition of robustness, i.e., the choice of the robustness measure that is generally expressed by the combination of statistical properties of the objective function. Several definitions of measures of robustness have been proposed in literature [10, 11, 18, 47] and the weighted sum of both the mean and the standard deviation of the objective function is often considered. The tradeoff between these two statistical measures gives rise to a final design that is less sensitive to parameters variations, i.e., a kind of robust design.

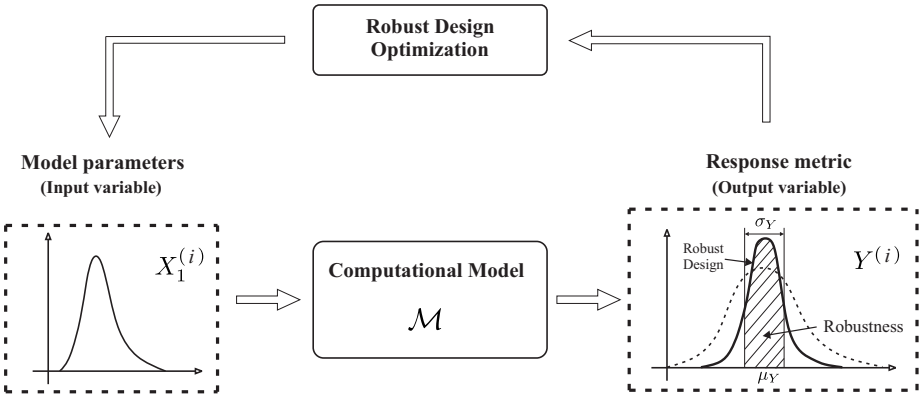


Figure 2 General overview of the robust design optimization procedure.

3.3 Robust topology optimization

In order to increase the optimal design robustness, the concept of robust optimization described in section 3.2 can be applied to TO. This possibility is addressed in this paper where variabilities in the external loading acting on the structure of interest are taken into account. Thus, the force vector and the compliance function become random objects, more precisely, a random vector $\mathbf{F}(\theta)$ and a random variable $C(\boldsymbol{\rho}, \theta)$, both defined on the probability space $(\Theta, \mathcal{F}, P)$.

For the sake of computational implementation, these objects are parametrized by a set of ν_{rv} suitable random variables that are lumped into the germ $\boldsymbol{\xi}(\theta) = \big(\xi_1(\theta), \xi_2(\theta), \cdots, \xi_{\nu_{rv}}(\theta)\big)$ so that force vector and compliance can be expressed as $\mathbf{F}(\boldsymbol{\xi})$ and $C(\boldsymbol{\rho}, \boldsymbol{\xi})$.

A straightforward measure of structural performance (robustness of the objective function) in RDO framework is given by the mean of the compliance $\mu_{C(\boldsymbol{\rho},\boldsymbol{\xi})}$. However, the final design may still be sensitive to the fluctuation due to external loading uncertainties and this may give rise to the need for a more robust design [20]. Then, the standard deviation of the compliance $\sigma_{C(\boldsymbol{\rho},\boldsymbol{\xi})}$ is also introduced into the formulation of the structural performance measure $\tilde{C}$, so that it is a linear combination between the mean and standard deviation of the random compliance $C(\boldsymbol{\rho}, \boldsymbol{\xi})$. By combining these two statistics it is possible to improve the design by minimizing the variability of the structural performance, satisfying the volume constraint.

This procedure, called robust topology optimization (RTO), can be mathematically formulated as

$$\begin{aligned} \min_{\boldsymbol{\rho}} \;\; & \tilde{C}(\boldsymbol{\rho}) = \mu_{C(\boldsymbol{\rho},\boldsymbol{\xi})} + w\, \sigma_{C(\boldsymbol{\rho},\boldsymbol{\xi})}, \\ s.t. \;\; & V(\boldsymbol{\rho}) = \sum_{e=1}^{N} \rho_e \, |\Omega^e| \leq v_S, \end{aligned} \tag{38}$$

which depends on the weight $w \geq 0$ and on the random displacement map $\mathbf{U}(\boldsymbol{\rho}, \boldsymbol{\xi})$, implicitly defined by the random equilibrium equation

$$\boldsymbol{K}(\boldsymbol{\rho})\, \mathbf{U}(\boldsymbol{\rho}, \boldsymbol{\xi}) = \mathbf{F}(\boldsymbol{\xi}). \tag{39}$$

The RTO problem defined in (38) can be solved by considering non-intrusive methods for stochastic computation. The basic idea of non-intrusive methods is to use a set of deterministic model evaluations to construct an approximation of the desired (random) output response. The deterministic evaluations are obtained for a finite set of realizations of parameter $\boldsymbol{\xi}$ with the aid of a deterministic solver (e.g. finite element code), that is used as a black box. Thus, non-intrusive methods offer a very simple way to propagate uncertainties in complex models, such as structural optimization, where only deterministic solvers are available. In this study the focus is on two non-intrusive techniques, namely, MC simulation [30, 46] and gPC expansion [63, 23].

3.4 Low-order statistics for compliance

Monte Carlo (MC) method is one of the simplest crude techniques for stochastic simulation and may be used to construct mean-square consistent and unbiased estimations (approximations) — see [30] for details — for $\mu_C = \mu_{C(\boldsymbol{\rho},\boldsymbol{\xi})}$ and $\sigma_C = \sigma_{C(\boldsymbol{\rho},\boldsymbol{\xi})}$, respectively defined by

$$\widehat{\mu}_C = \frac{1}{\nu_{mc}} \sum_{n=1}^{\nu_{mc}} C_n, \tag{40}$$

and

$$\widehat{\sigma}_C = \left(\frac{1}{\nu_{mc} - 1} \sum_{n=1}^{\nu_{mc}} \left(C_n - \widehat{\mu}_C\right)^2 \right)^{1/2}, \tag{41}$$

where $C_n = C(\boldsymbol{\rho}, \boldsymbol{\xi}_n)$, $\boldsymbol{\xi}_n$ is the n-th realization of the germ $\boldsymbol{\xi}$ and ν_{mc} denotes the number of MC realizations.

Despite its simplicity, the slow convergence rate of MC method ($\sim 1/\sqrt{\nu_{mc}}$) usually makes it a very expensive stochastic solver in terms of computational cost, particularly for TO problems, where a large number of deterministic model resolutions needs to be obtained to achieve an adequate response characterization. For this reason, a gPC procedure for low-order statistics estimation is also considered in this work.

Using the gPC approach, an spectral representation of the compliance function can be written as

$$C(\boldsymbol{\rho}, \boldsymbol{\xi}) = \sum_{n=0}^{+\infty} c_n(\boldsymbol{\rho})\, \psi_n(\boldsymbol{\xi}), \tag{42}$$

in a way that, because of properties $E\{\psi_0\} = 1$ and $E\{\psi_n\} = 0,\ n \geq 1$, the mean value of $C(\boldsymbol{\rho}, \boldsymbol{\xi})$ writes as

$$\mu_C = E\left\{C(\boldsymbol{\rho}, \boldsymbol{\xi})\right\} = c_0(\boldsymbol{\rho}), \tag{43}$$

where an approximation for the PCE coefficient c_0 is obtained from the linear regression (26). This procedure induces a Gaussian quadrature estimation of μ_C, defined by the estimator

$$\widehat{\mu}_C^{\,'} = \sum_{j=1}^{\nu_{gq}} W_j\, C_j, \tag{44}$$

where $C_j = C(\boldsymbol{\rho}, \boldsymbol{\xi}_j)$ corresponds to the evaluation of the compliance at the Gauss points and the quadrature weights $W_j = \Psi^{\dagger}_{1j}$ are given by the first line entries of $\boldsymbol{\Psi}^{\dagger} = (\boldsymbol{\Psi}^T \boldsymbol{\Psi})^{-1} \boldsymbol{\Psi}^T$, the pseudoinverse of the $\nu_{gq} \times \nu_{pc}$ regression matrix $\boldsymbol{\Psi}$.

By definition, the standard deviation of compliance is written as

$$\sigma_C = \left(E\left\{ C(\boldsymbol{\rho}, \boldsymbol{\xi})^2 \right\} - E\left\{ C(\boldsymbol{\rho}, \boldsymbol{\xi}) \right\}^2 \right)^{1/2}, \tag{45}$$

so that a procedure similar to that used to construct the estimator of Eq.(44) can be adopted now to propose

$$\widehat{\sigma}_C^{\,\prime} = \left(\sum_{j=1}^{\nu_{gq}} W_j \, C_j^2 - \left(\widehat{\mu}_C^{\,\prime} \right)^2 \right)^{1/2}, \tag{46}$$

as an estimator for σ_C.

The gPC-based estimators defined by Eqs.(44) and (46) provide a very accurate and efficient framework for estimation of the compliance low-order statistics, that demands a small number of deterministic model evaluations, once in practice $\nu_{gq} \ll \nu_{mc}$.

3.5 Sensitivity analysis

The partial derivative of the objective function $\tilde{C}$, defined in the optimization problem (38), with respect to the element density function ρ_e is given by

$$\frac{\partial \tilde{C}}{\partial \rho_e} = \frac{\partial \mu_C}{\partial \rho_e} + w \, \frac{\partial \sigma_C}{\partial \rho_e}, \tag{47}$$

where the partial derivatives on the right hand side can be approximated, via crude MC, with the aid of the estimators

$$\frac{\partial \mu_C}{\partial \rho_e} \approx \widehat{\frac{\partial \mu_C}{\partial \rho_e}} = \frac{1}{\nu_{mc}} \sum_{n=1}^{\nu_{mc}} \frac{\partial C_n}{\partial \rho_e} \tag{48}$$

and

$$\frac{\partial \sigma_C}{\partial \rho_e} \approx \widehat{\frac{\partial \sigma_C}{\partial \rho_e}} = \frac{1}{(\nu_{mc} - 1)\, \widehat{\sigma}_C} \left(\left(\sum_{n=1}^{\nu_{mc}} C_n \, \frac{\partial C_n}{\partial \rho_e} \right) - \nu_{mc} \, \widehat{\mu}_C \, \widehat{\frac{\partial \mu_C}{\partial \rho_e}} \right). \tag{49}$$

However, from the point of view of computational cost, it is more efficient to obtain these sensitivity coefficients using the gPC estimators, i.e.

$$\frac{\partial \mu_C}{\partial \rho_e} \approx \widehat{\frac{\partial \mu_C}{\partial \rho_e}}^{\,\prime} = \sum_{j=1}^{\nu_{gq}} W_j \, \frac{\partial C_j}{\partial \rho_e} \tag{50}$$

and

$$\frac{\partial \sigma_C}{\partial \rho_e} \approx \widehat{\frac{\partial \sigma_C}{\partial \rho_e}}^{\,\prime} = \frac{1}{\widehat{\sigma}_C^{\,\prime}} \left(\left(\sum_{j=1}^{\nu_{gq}} W_j \, C_j \, \frac{\partial C_j}{\partial \rho_e} \right) - \widehat{\mu}_C^{\,\prime} \, \widehat{\frac{\partial \mu_C}{\partial \rho_e}}^{\,\prime} \right), \tag{51}$$

obtained from Eqs.(44) and (46) by differentiation with respect to ρ_e.

3.6 Algorithm for robust topology optimization

The results obtained from the TO algorithm, i.e., the compliance and sensitivities, are used to compute statistical measures in a non-intrusive way. Therefore, the RTO algorithm, for problems with uncertain loading, can be described as follows:

1. Topology Optimization Data: define finite element model, set optimizer and underlying numerical and control parameters;
2. Stochastic Model: parametrize aleatory objects with a set of independent random variables defined by the germ $\boldsymbol{\xi}$. Choose an appropriate family of orthogonal polynomials, define weight factor w and gPC order p_{pc};
3. Objective Function
   - for each germ realization $\boldsymbol{\xi}_n$ perform finite element analysis using Eq.(39) and compute compliance sensitivities with Eq.(36);
   - Compute gPC coefficients from Eq.(26);
   - Compute statistical estimates for mean and standard deviation with aid of Eqs.(44) and (46);
   - Compute the sensitivity of the objective function from Eq.(47).
4. Constraint Function: compute volume constraint using Eq.(34) and its sensitivity with Eq.(37);
5. Update the design variables $\boldsymbol{\rho}$ according to the optimizer. Repeat from step 3 until convergence is achieved;

A flowchart of the proposed RTO algorithm is depicted in Figure 3.

4 Numerical examples

The effectiveness of the proposed gPC RTO algorithm is addressed in this section by means of a study that considers bidimensional mechanical systems subjected to uncertain loads. The goal is to show that different statistical responses can be obtained when using the proposed gPC RTO design algorithm and a non-robust design strategy, where TO is done first (deterministically) and the propagation of uncertainties is computed later, considering the deterministic optimized topology.

For the sake of accuracy verification, a reference crude Monte Carlo RTO solution is employed. This comparison allows one the verify the accuracy of the statistical measures obtained with the proposed gPC approach. The influence of the weight factor in the robust design is also addressed, as well as the different effects that are observed when a random load is treated as a random variable or a random field.

For the examples presented in the following section, consistent units are used.

4.1 Cantilever beam design

This first example consists of a simple cantilever beam subjected to a pair of vertical loads, with uncertain magnitudes, applied at the two right edge corners, as illustrated in Figure 4(a). This problem has been studied by Wu et al.[61].

The vertical and horizontal dimensions of the structure are 30 and 60 units of length, respectively. The structure is composed of an isotropic material with

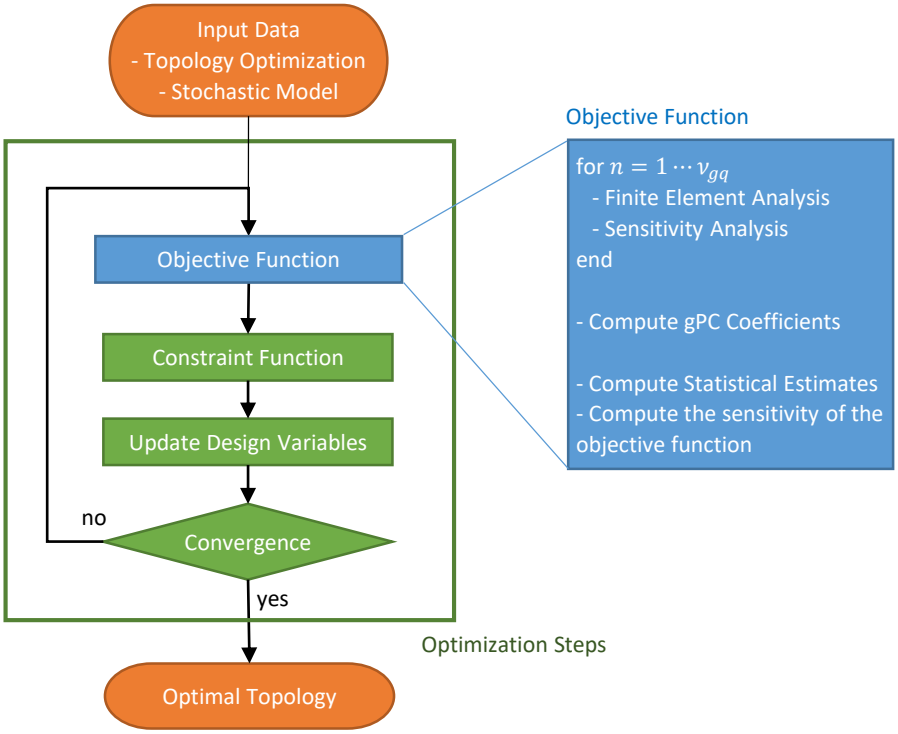
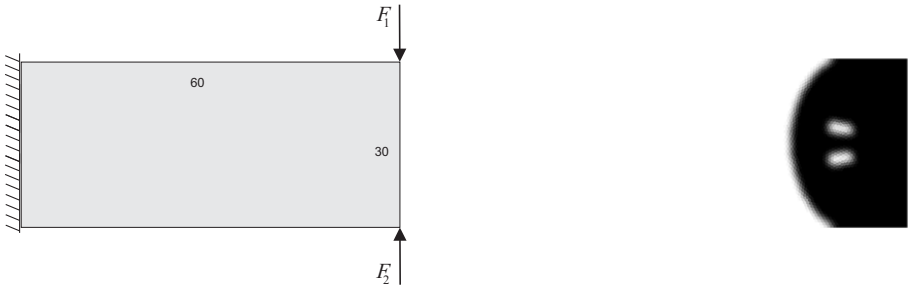


Figure 3 General flow chart of the gPC RTO integrated procedure.



(a) (b)

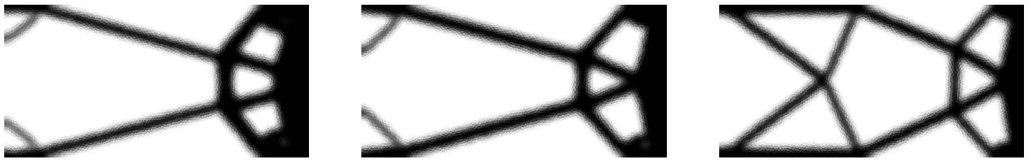
Figure 4 Cantilever beam structure: (a) original configuration, (b) non-robust TO design.

Young modulus $E_0 = 1$ and Poisson ratio $\nu = 0.3$. For the void material an elastic modulus value equal to $E_{min} = 10^{-9}$ is employed. The prescribed volume fraction of material is set as 0.3, the filter radius as 1.5, the penalization factor 3, and the design domain is discretized by means of a polygonal mesh with $N = 7,200$ finite elements. The nominal (deterministic) configuration for this problem adopts the magnitude of the two vertical forces as $F_1 = F_2 = 1$, respectively.

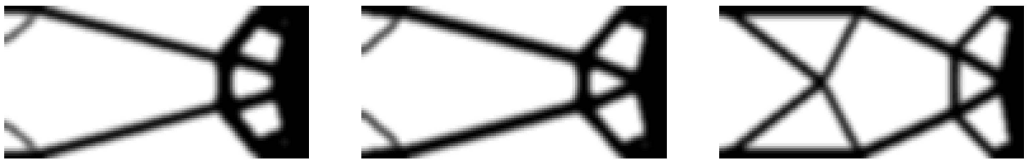
On the other hand, in the stochastic case, magnitudes of the forces are assumed to be uncertain and modeled by independent random variables $\theta \in \Theta \mapsto F_1(\theta) \in \mathbb{R}$ and $\theta \in \Theta \mapsto F_2(\theta) \in \mathbb{R}$, both defined on a suitable probability space $(\Theta, \mathcal{F}, P)$. For the sake of simplicity, but being consistent with the physics of the mechanical problem, it is assumed that these two random variables are uniformly distributed on the same positive support $\texttt{Supp}\, F = [F_{min}, F_{max}] \subset (0, +\infty)$. Three numerical studies are conducted in this example, where $\texttt{Supp}\, F$ is chosen as $[F_{min}, F_{max}] = [0.95, 1.05]$, $[F_{min}, F_{max}] = [0.9, 1.1]$ and $[F_{min}, F_{max}] = [0.8, 1.2]$. Note that these intervals correspond to symmetrical variabilities of up to 5%, 10% and 20% around the mean values $\mu_{F_1} = \mu_{F_2} = 1$, respectively.

The non-robust TO, obtained using the `PolyTop` with MMA optimizer, is shown in Figure 4(b). The lack of material on the left side of the cantilever is due to the two forces of equal magnitudes applied in opposite directions. Therefore, the stress in the cantilever is distributed only on the right side of the domain. However, to avoid instability (displacements going to infinity), a minimum value of elastic modulus E_{min} is used.

In order to perform the gPC RTO one needs to define the germ $\boldsymbol{\xi} = (F_1, F_2)$, which is over the region $[F_{min}, F_{max}] \times [F_{min}, F_{max}] \subset (0, +\infty) \times (0, +\infty)$, so that $\nu_{rv} = 2$. In this case the optimal base for gPC expansion is given by the Legendre polynomials [63]. For the three different types of uniform distribution considered, a weight factor $w = 1$ is employed, together with an expansion of order $p_{pc} = 5$ (so that $1 + \nu_{pc} = 21$)(this value was heuristically chosen to ensure the stochastic convergence.). A total number of $\nu_{gq} = 36$ collocation points is used to generate realizations of $\boldsymbol{\xi} = (F_1, F_2)$. To check the accuracy of the gPC RTO strategy, the same problem is addressed using the MC simulation with $\nu_{mc} = 10^4$ scenarios of loading magnitudes, a reference result dubbed MC RTO.



(a) gPC RTO design



(b) MC RTO design

Figure 5 Optimized topologies for the cantilever beam using gPC RTO and MC RTO designs, for uniform distributions over the intervals $[F_{min}, F_{max}] = [0.95, 1.05]$ (left), $[F_{min}, F_{max}] = [0.9, 1.1]$ (center) and $[F_{min}, F_{max}] = [0.8, 1.2]$ (right).

In Figure 5 the reader can see the optimum topologies obtained by gPC RTO (top) and MC RTO (bottom), for different support of the random variable F. The topologies shown in Figure 5 are different from the deterministic counterparts in Figure 4(b) – some extra members can be observed on the left side of the structure – for different levels of uncertainties (length of $\texttt{Supp}\, F$). As the level of uncertainty increases, more members appear in the final topology. Finally, the robust designs using MC simulation present equivalent topologies and statistical measures, which demonstrates the accuracy of the proposed gPC RTO approach.

Table 1 compares statistical estimates for the compliance expected value μ_C and standard deviation σ_C, in the cases of robust and non-robust design. Remember that, in this context, non-robust design means first optimizing the topology via classical (deterministic) TO and then using MC simulation to propagate the loading uncertainties through the mechanical system. A good agreement between robust strategies based on gPC and MC is noted, as well as that the statistical measures for the non-robust design tend to approach infinity, since there is no connection between the left and right sides of the domain. It is also worth noting that, while the MC RTO needs 10^4 evaluations of the compliance function, the gPC RTO only needs 36 evaluations. This difference of three orders of magnitude demonstrates the efficiency of the gPC RTO implementation.

Table 1 Low-order statistics of cantilever beam compliance for robust and non-robust TO strategies.

$\texttt{Supp}\, F$	gPC RTO		MC RTO		Non-robust TO	
	μ_C	σ_C	μ_C	σ_C	μ_C	σ_C
$[0.95, 1.05]$	21.4	1.2	21.4	1.2	5.7 E7	6.7 E7
$[0.90, 1.10]$	23.5	2.9	23.4	2.8	2.3 E8	2.7 E8
$[0.80, 1.20]$	29.4	7.7	29.4	7.6	9.1 E8	1.1 E9

4.2 Michell type structure

In this second example RTO is performed on a simple Michell type structure considering three loads, with uncertain directions, applied at the bottom edge of the two dimensional system, as illustrated in Figure 6(a).

The length and height of the structure are equal to 120 and 50 units, respectively. The design domain is discretized with a polygonal mesh with $N = 12,000$ finite elements, and all other parameters are the same as in the first example. For the deterministic case, magnitudes and directions of the three forces are defined as $F_1 = 1$, $F_2 = 2$, $F_3 = 1$, and $\alpha_1 = \alpha_2 = \alpha_3 = -90$, respectively.

Meanwhile, on the stochastic case, the forces directions are modeled as the independent and identically distributed random variables $\theta \in \Theta \mapsto A_1(\theta) \in \mathbb{R}$, $\theta \in \Theta \mapsto A_2(\theta) \in \mathbb{R}$ and $\theta \in \Theta \mapsto A_3(\theta) \in \mathbb{R}$. Three scenarios of probabilistic distribution are analyzed: (i) Normal, (ii) Uniform, and (iii) Gumbel. For the Normal and Gumbel distributions, mean values are assumed to be equal to the nominal values of α_1, α_2 and α_3, with all the standard deviations equal to 10. In

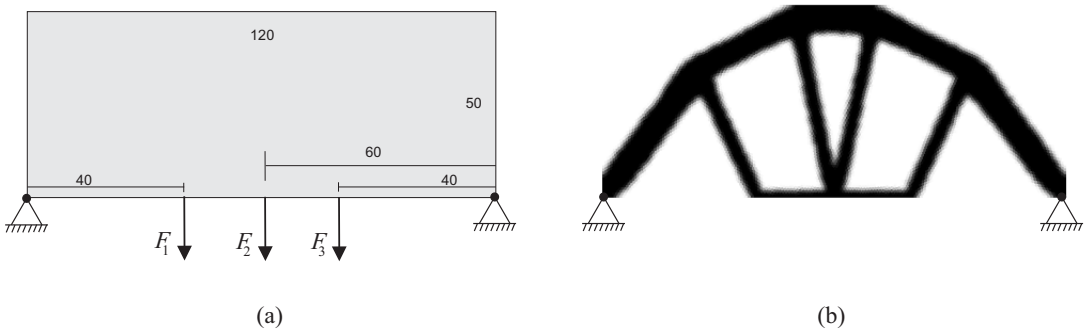


Figure 6 Michell type structure: (a) original configuration, (b) non-robust TO design.

the Uniform case, the three supports are defined by the interval $[A_{min}, A_{max}] = [-100, -80]$. The probability density functions of these distributions are illustrated in Figure 7.

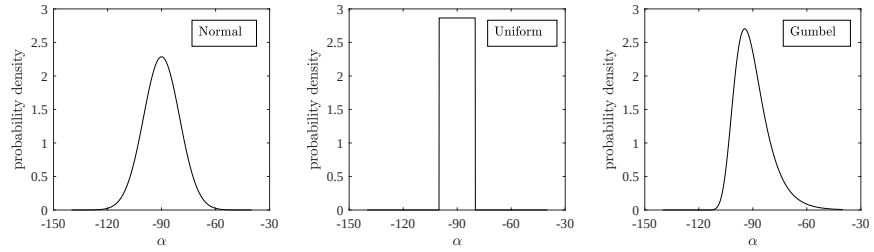
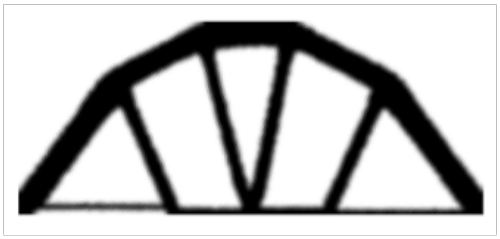


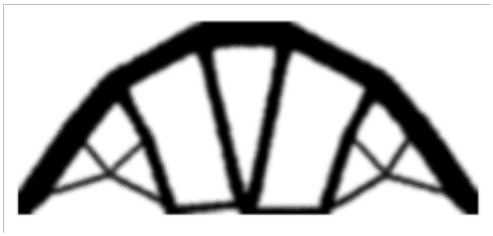
Figure 7 Probability distributions for the loads angles: normal (left), uniform (center) and Gumbel (right).

Now the germ is defined as $\boldsymbol{\xi} = (A_1, A_2, A_3)$, thus $\nu_{rv} = 3$, and the family of orthogonal polynomials (basis) is chosen according to the germ support. For simplicity, Hermite polynomials are used in the case of Gaussian or Gumbel parameters, while Legendre polynomials are the option when the germ is uniform distributed. Employing gPC RTO with an expansion of order $p_{pc} = 5$ (thus $1 + \nu_{pc} = 56$) total number of $\nu_{gq} = 216$ collocation points and and weight factor value $w = 1$, one obtains the robust designs shown in Figure 8, where connections at fixed points are created to balance the horizontal components of non-vertical forces. Note that the non-robust design in Figure 6(b) only presents four bars connected at the forces application points, no connection at the joints can be seen. This occurs because the forces are always vertical. However, when gPC RTO design is used, there are connections at the joints, because the angle variability induces horizontal force components.

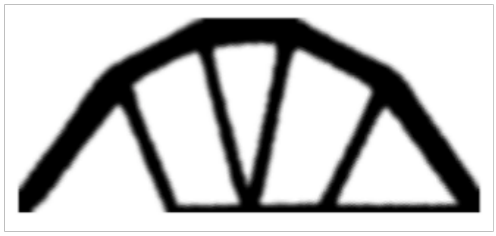
The statistical results of the robust design compared with the non-robust counterpart can be appreciated in Figure 9 and Table 2, which show the compliance probability densities and their low order statistics, respectively, for the different distributions considered in the force angle. One can observe from these simulation



(a) Normal



(b) Uniform



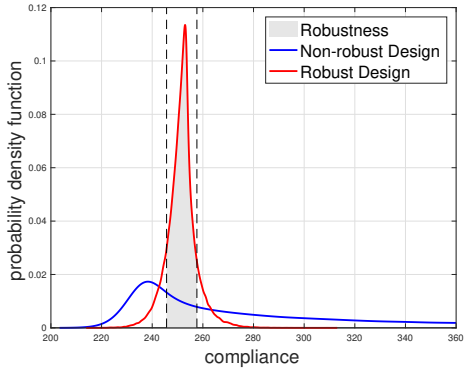
(c) Gumbel

Figure 8 Optimized topologies for the Michell type structure using gPC RTO design, with different probability distributions for load angle: (a) Normal, (b) Uniform and (c) Gumbel.

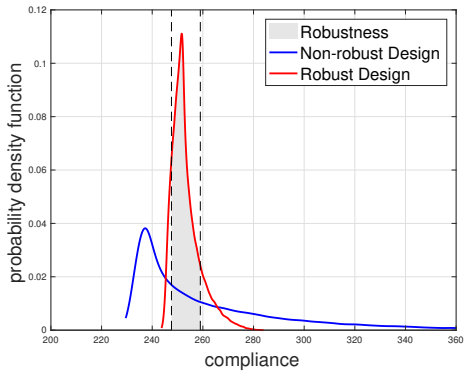
results that the range variability of compliance is reduced, which implies that the robust design is less sensitive to loading uncertainties than its non-robust counterpart. As shown in Figure 8, the final topologies are symmetric for the normal and uniform distributions but is asymmetric for the Gumbel distribution.

Table 2 Low-order statistics of the compliance for the Michell type structure using robust and non-robust TO strategies.

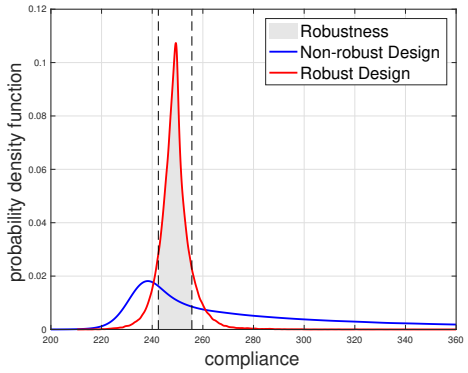
distribution	gPC RTO		Non-robust TO	
	μ_C	σ_C	μ_C	σ_C
Normal	251.6	6.0	314.2	113.3
Uniform	253.3	5.7	262.7	33.3
Gumbel	249.1	6.7	312.5	128.9



(a) Normal

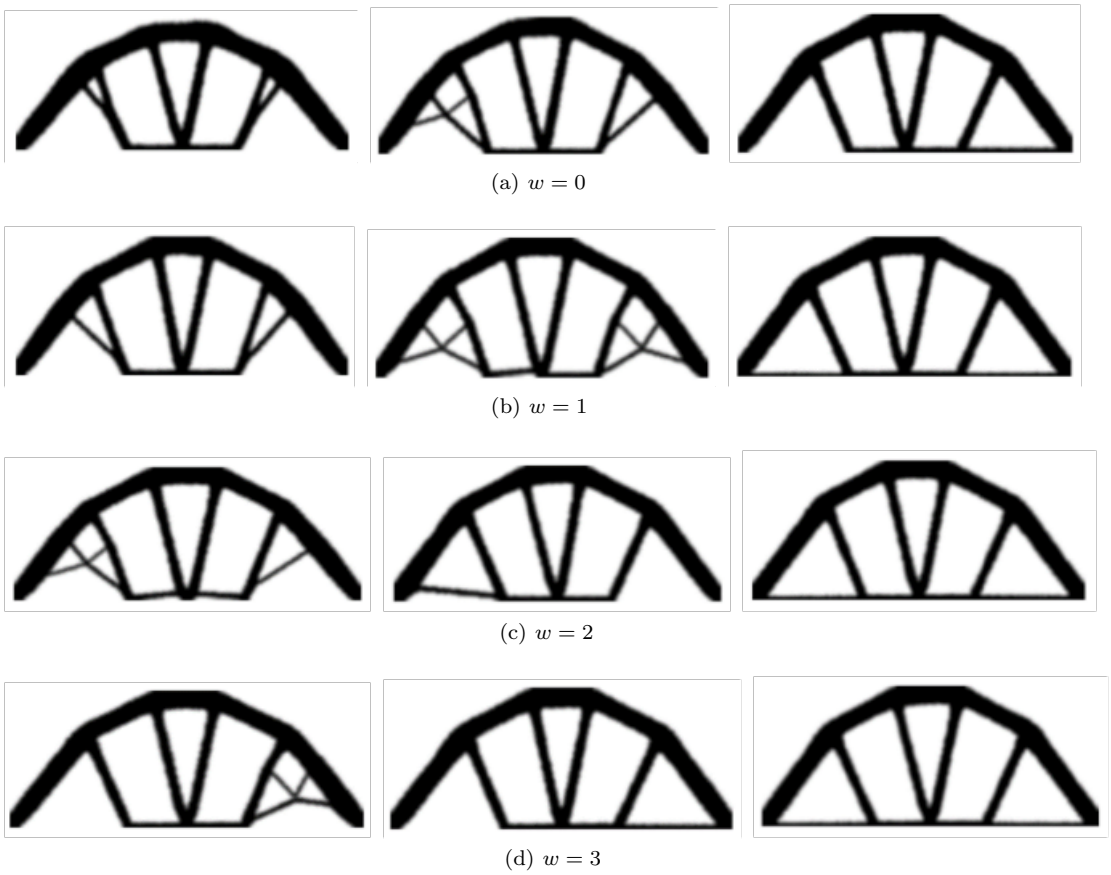


(b) Uniform



(c) Gumbel

Figure 9 Probability density function of the compliance for the Michell type structure using non-robust and gPC RTO robust design, with different probability distributions for load angle: (a) Normal, (b) Uniform and (c) Gumbel.



(a) $w = 0$

(b) $w = 1$

(c) $w = 2$

(d) $w = 3$

Figure 10 Optimized topologies for the Michell type structure using gPC RTO strategy, for different values of weight w and different uniform distributions for the angle: $[-95, -85]$ (left), $[-100, -80]$ (middle) and $[-110, -70]$ (right).

In the second analysis for this example, the influence of the weighting factor in the robust optimization process is addressed. The aim is to minimize the variability by increasing the value of w, because this factor is directly related to the standard deviation term on the objective function.

Three different uniform distributions are considered for the random angle of the force and their supports are respectively defined by the intervals $[A_{min}, A_{max}] = [-95, -85]$, $[A_{min}, A_{max}] = [-100, -80]$ and $[A_{min}, A_{max}] = [-110, -70]$. The gPC RTO design strategy is employed for $w \in \{0, 1, 2, 3\}$, generating the optimal topologies shown in Figure 10. According to Table 3, all the designs shown in Figure 10 present significant lower expected compliance and standard deviation values when compared to the non-robust solution. The highest values of standard deviation are obtained using $w = 0$, since we are minimizing only the expected compliance. For $w > 0$, both expected compliance and its standard deviation contribute to the objective function and we can observe that as the value of w increases, the standard deviation decreases. Based on the

numerical experiments presented in Table 3, we recommend the value $w = 3$, for practical use, because it leads to the best values of standard deviation with only a slight change in the expected compliance values.

Table 3 Low-order statistics of the compliance for the Michell type structure using gPC RTO, with different force angles distributions and different weight factors.

		Supp A					
		$[-95, -85]$		$[-100, -80]$		$[-110, -70]$	
	w	μ_C	σ_C	μ_C	σ_C	μ_C	σ_C
gPC RTO	0	241.8	5.2	256.0	10.6	249.0	10.2
gPC RTO	1	247.2	4.3	253.3	5.7	249.2	6.4
gPC RTO	2	253.0	3.1	249.7	4.0	250.0	6.0
gPC RTO	3	248.9	2.4	247.0	2.9	250.1	5.6
Non-robust TO	-	364.4	14.2	366.1	28.4	373.0	56.9

4.3 2D bridge structure

This last example corresponds to a simple bridge structure subjected to an uncertain distributed loading at the top edge, as illustrated in Figure 11(a). The nominal load is uniform throughout the structure, with magnitude per unit of length equal to $F = 1$.

For the stochastic case, the load magnitude per unit of length in each point is assumed to be a Gaussian random field $(\theta, x) \in \Theta \times [0, l] \mapsto F(\theta, x) \in \mathbb{R}$ with correlation function

$$\mathcal{K}_F(x, x') = \sigma_F, \tag{52}$$

such that the loads at any pair of points x, x' are fully correlated. The mean and standard deviation of the random field $F(\theta, x)$ are assumed as $\mu_F = 1$ and $\sigma_F = 0.3$, respectively.

For the optimization process, the prescribed volume fraction of material is set as 0.3, the filter radius is set as 3, the penalization factor 3, and the design domain is discretized with a polygonal mesh with $N = 10,000$ finite elements. The non-robust TO of the 2D bridge, performed using `PolyTop` with MMA optimizer, is shown in Figure 11(b). Furthermore, the first two rows of finite elements on the top of structure are fixed during the optimization process, to ensure that the bridge remains attached to the loading conditions. Allowing the final results to be more realistic. It is observed in Figure 11(b) that the non-robust design leads to a final topology which is similar to the classical case of a 2D bridge under an uniformly distributed load.

For the purpose of numerical computation, the random field $F(\theta, x)$ is discretized by means of $\boldsymbol{\xi} = (F_1)$, a single Gaussian random variable for which low-order statistics are the same as for the random field. The gPC RTO design is obtained using an expansion of order $p_{pc} = 5$ (with $1 + \nu_{pc} = 6$) and a total number of $\nu_{gq} = 6$ collocation points for Hermite orthogonal polynomials, and weight factor values $w \in \{0, 1, 2, 3\}$.

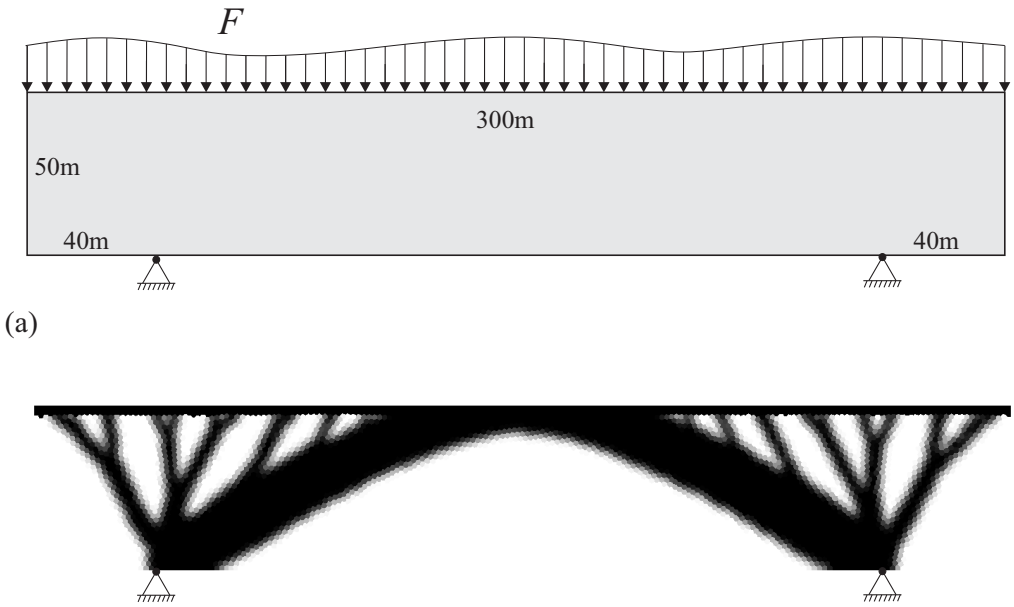


Figure 11 2D Bridge structure: (a) original configuration, (b) non-robust RO design.

The final results are shown in Figure 12, where one can observe that some bars connected at the bottom of the bridge are different from those of the non-robust case in Figure 11(b). Moreover, as the value of w increases, the structure presents a more robust physical form, which represents a consistent result, because the standard deviation of the compliance is being forced to be smaller. The corresponding mean value and standard deviation of the compliance function, for the different values of w employed, are given in Table 4.

Table 4 Low-order statistics of the compliance for a 2D bridge using gPC RTO and different weight factors.

w	μ_C	σ_C
0	5.4443 E5	3.0666 E5
1	5.4481 E5	3.0657 E5
2	5.4462 E5	3.0646 E5
3	5.4455 E5	3.0642 E5

As a second analysis, the random load $F(\theta, x)$ is assumed to have the same low-order statistics as before, but an exponentially decaying correlation function

$$\mathcal{K}_F(x, x') = \sigma_F \exp\left(-\frac{|x - x'|}{l_{corr}}\right), \tag{53}$$

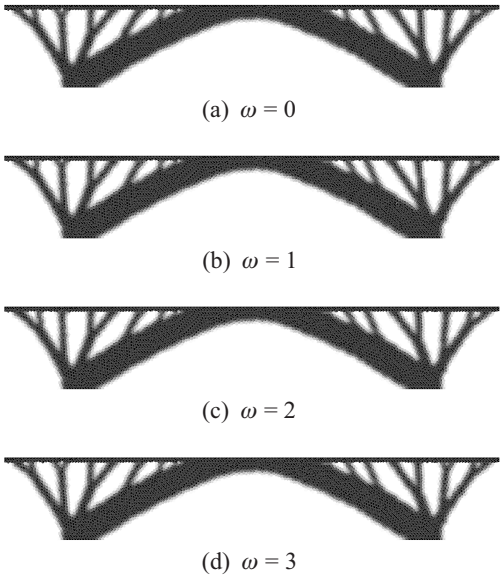


Figure 12 Robust design for the 2D bridge structure with fully correlated distributed load, for different values of weight w.

where l_{corr} is a correlation length for the random field. Note that, by this assumption, the loads at any two points x, x' in the 2D bridge are partially correlated. If the correlation length is increased, a strong correlation is obtained between the points x, x', so that $l_{corr} = \infty$ implies a perfectly correlated random field — the previous case where the field depends on a single random variable. On the other hand, when $l_{corr} = 0$, the random field is completely uncorrelated — many independent random variables are necessary for an accurate computational representation. In order to avoid the two limit cases, $l_{corr} = 120$ is chosen.

In terms of computational representation for numerical calculations, the random field $F(\theta, x)$ is discretized with the aid of Karhunen–Loève expansion described in section 2.2. The number of terms in this expansion is chosen in a heuristic way, seeking to satisfy the criterion presented in (16). A good compromise between accuracy and computational efficiency is obtained with $\nu_{kl} = 7$. Therefore, the germ is $\boldsymbol{\xi} = (F_1, F_2, \cdots, F_{\nu_{rv}})$, a set of $\nu_{rv} = 7$ independent Gaussian random variables for which low-order statistics are the same as for the random field. Then, for this case we use a total number of $\nu_{gq} = 279936$ collocation points.

A comparison between non-robust and gPC RTO design, for $w = 1$ and the different types of distributed load considered, are shown in Figure 13. The difference between the three obtained topologies is very clear, and can also be appreciated in Table 5, which shows the low-order statistics of the compliance in all cases analyzed.

This example clearly shows that the nature of the distributed load has a significant effect on the RTO. Also from Table 5, it is possible to see that the compliance low-order statistics for a 2D bridge under a distributed load, emulated by a partially correlated random field, are smaller than those for a fully correlated field.

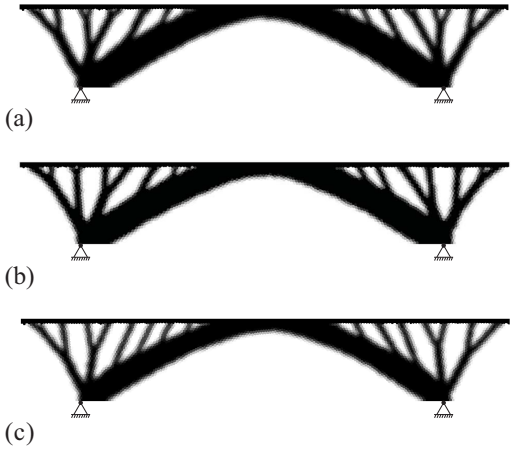


Figure 13 Optimized topologies for the 2D bridge structure: (a) non-robust TO with fully correlated load, (b) gPC RTO with fully correlated load, (c) gPC RTO with partially correlated load.

Table 5 Low-order statistics of the compliance for a 2D bridge considering different design scenarios.

Non-robust TO		RTO full corr		RTO partial corr	
μ_C	σ_C	μ_C	σ_C	μ_C	σ_C
5.449 E5	3.076 E5	5.448 E5	3.066 E5	2.361 E5	9.708 E4

5 Conclusions

In the present paper RTO problem has been formulated and solved by means of an optimization procedure which integrates a classical TO algorithm with a stochastic spectral expansion based on gPC. Monte Carlo simulation is used to verify the accuracy and efficiency of the proposed methodology. This approach is introduced to reduce the variability due to uncertain loadings applied to the mechanical structure of interest. The objective function of the robust problem is defined as the weighted sum of the mean and standard deviation of the compliance, and it can be computed by considering a number of additional load cases. This makes the RTO computationally tractable and accessible by any TO algorithm. Furthermore, the gPC is compatible with RTO for computing the statistical measures of the compliance. The numerical examples presented here show a substantial benefit and exhibits topology changes within their design domains compared with their deterministic counterpart. The optimal topology configurations confirm that the uncertainty parameters might change the deterministically obtained optimal topologies. The proposed methodology allows to obtain approximate outcomes with a much lower computational cost than that associated with Monte Carlo simulation, which makes it attractive, particularly in the context of structural topology optimization. Moreover, when using random load fields, the results show different topologies because the forces are correlated, i.e., each force

depends on the other and therefore, their interactions with the structure have significant effects on the robust design. The limitation of the gPC can be observed when a large number of random variables is used to parametrize the stochastic model, since in this case a substantial number of terms is necessary to construct the expansion, and, consequently, the computational cost increases significantly with the dimension. This is often referred to as the curse of dimensionality, and it can be reduced using adaptive techniques such as the adaptive sparse grid.

Acknowledgments

NC acknowledges the financial support from the Group of Technology in Computer Graphics (Tecgraf/PUC-Rio), Rio de Janeiro, Brazil. AP and IFMM acknowledge the financial support from the National Council for Scientific and Technological Development (CNPq) under projects 312280/2015-7 and 309708/2015-0, respectively. AP and ACJr are thankful for the support from Carlos Chagas Filho Research Foundation of Rio de Janeiro State (FAPERJ) under grants E-26/203.189/2016, E-26/010.002.178/2015 and E-26/010.000.805/2018. The information provided in this paper is the sole opinion of the authors and does not necessarily reflect the views of the sponsoring agencies.

References

1. Andreasen CS, Sigmund O (2013) Topology optimization of fluid–structure-interaction problems in poroelasticity. Computer Methods in Applied Mechanics and Engineering 258:55–62, DOI https://doi.org/10.1016/j.cma.2013.02.007
2. Antonietti P, Bruggi M, Scacchi S, Verani M (2017) On the virtual element method for topology optimization on polygonal meshes: A numerical study. Computers & Mathematics with Applications 74(5):1091 – 1109, DOI https://doi.org/10.1016/j.camwa.2017.05.025, URL `http://www.sciencedirect.com/science/article/pii/S0898122117303309`, sI: SDS2016 – Methods for PDEs
3. Asadpoure A, Tootkabonia M, Guest J (2011) Robust topology optimization of structures with uncertainties in stiffness - Application to truss structures. Computers & Structures 89:1031–1041, DOI https://doi.org/10.1016/j.compstruc.2010.11.004
4. Atkinson KE (2009) The Numerical Solution of Integral Equations of the Second Kind, reissue edn. Cambridge University Press
5. Banichuk N, Neittaanmäki P (2010) Structural Optimization with Uncertainties. Springer Netherlands
6. Bellizzi S, Sampaio R (2012) Smooth decomposition of random fields. Journal of Sound and Vibration 331:3509–3520, DOI https://doi.org/10.1016/j.jsv.2012.03.030
7. Bendsøe MP, Kikuchi N (1988) Generating optimal topologies in structural design using a homogenization method. Computer Methods in Applied Mechanics and Engineering 71:197–224
8. Bendsøe MP, Sigmund O (2004) Topology Optimization: Theory, Methods, and Applications. Springer-Verlag Berlin Heidelberg

9. Betz W, Papaioannou I, Straub D (2014) Numerical methods for the discretization of random fields by means of the Karhunen–Loève expansion. Computer Methods in Applied Mechanics and Engineering 271:109–129, DOI https://doi.org/10.1016/j.cma.2013.12.010
10. Beyer HG, Sendhoff B (2007) Robust optimization – A comprehensive survey. Computer Methods in Applied Mechanics and Engineering 196:3190–3218, DOI https://doi.org/10.1016/j.cma.2007.03.003
11. Birge J, Louveaux F (2011) Introduction to Stochastic Programming. Springer-Verlag New York
12. Brezis H (2010) Functional Analysis, Sobolev Spaces and Partial Differential Equations. Springer-Verlag New York
13. Bruggi M (2008) On the solution of the checkerboard problem in mixed-FEM topology optimization. Computers & Structures 86:1819–1829, DOI https://doi.org/10.1016/j.compstruc.2008.04.008
14. Chen S, Chen W, Lee S (2010) Level set based robust shape and topology optimization under random field uncertainties. Structural and Multidisciplinary Optimization 41:507–524, DOI https://doi.org/10.1007/s00158-009-0449-2
15. Ciarlet PG (2013) Linear and Nonlinear Functional Analysis with Applications. SIAM
16. da Silva G, Cardoso E (2017) Stress-based topology optimization of continuum structures under uncertainties. Computer Methods in Applied Mechanics and Engineering 313:647–672, DOI https://doi.org/10.1016/j.cma.2016.09.049
17. Dapogny C, Faure A, Michailidis G, Allaire G, Couvelas A, Estevez R (2017) Geometric constraints for shape and topology optimization in architectural design. Computational Mechanics 59:933–965, DOI https://doi.org/10.1007/s00466-017-1383-6
18. Doltsinis I, Kang Z (2004) Robust design of structures using optimization methods. Computer Methods in Applied Mechanics and Engineering 193(23):2221–2237, DOI https://doi.org/10.1016/j.cma.2003.12.055
19. Duan XB, Li FF, Qin XQ (2015) Adaptive mesh method for topology optimization of fluid flow. Applied Mathematics Letters 44:40–44, DOI https://doi.org/10.1016/j.aml.2014.12.016
20. Dunning PD, Kim HA (2013) Robust topology optimization: Minimization of expected and variance of compliance. AIAA Journal 51:2656–2664, DOI https://doi.org/10.2514/1.J052183
21. Eldred M (2009) Recent advances in non-intrusive polynomial chaos and stochastic collocation methods for uncertainty analysis and design. In: 50th AIAA/ASME/ASCE/AHS/ASC Structures, Structural Dynamics, and Materials Conference, DOI https://doi.org/10.2514/6.2009-2274
22. Ghanem R (1999) Ingredients for a general purpose stochastic finite elements implementation. Computer Methods in Applied Mechanics and Engineering 168:19–34, DOI https://doi.org/10.1016/S0045-7825(98)00106-6
23. Ghanem R, Red-Horse J (2017) Polynomial Chaos: Modeling, Estimation, and Approximation, Springer International Publishing, pp 521–551. DOI https://doi.org/10.1007/978-3-319-12385-1_13
24. Ghanem RG, Spanos PD (2003) Stochastic Finite Elements: A Spectral Approach, 2nd edn. Dover Publications
25. Guest JK, Igusa T (2008) Structural optimization under uncertain loads and nodal locations. Computer Methods in Applied Mechanics and Engineering

198:116–124, DOI https://doi.org/10.1016/j.cma.2008.04.009
26. Hoshina TYS, Menezes IFM, Pereira A (2018) A simple adaptive mesh refinement scheme for topology optimization using polygonal meshes. Journal of the Brazilian Society of Mechanical Sciences and Engineering 40(7):348, DOI 10.1007/s40430-018-1267-5, URL https://doi.org/10.1007/s40430-018-1267-5
27. Jalalpour M, Guest JK, Igusa T (2013) Reliability-based topology optimization of trusses with stochastic stiffness. Structural Safety 43:41–49, DOI https://doi.org/10.1016/j.strusafe.2013.02.003
28. Keshavarzzadeh V, Fernandez F, Tortorelli DA (2017) Topology optimization under uncertainty via non-intrusive polynomial chaos expansion. Computer Methods in Applied Mechanics and Engineering 318:120–147, DOI https://doi.org/10.1016/j.cma.2017.01.019
29. Kim NH, Wang H, Queipo NV (2006) Efficient shape optimization under uncertainty using polynomial chaos expansions and local sensitivities. AIAA Journal 44:1112–1116, DOI https://doi.org/10.2514/1.13011
30. Kroese DP, Taimre T, Botev ZI (2011) Handbook of Monte Carlo Methods. Wiley
31. Kundu A, Adhikari S, Friswell M (2014) Stochastic finite elements of discretely parameterized random systems on domains with boundary uncertainty. International Journal for Numerical Methods in Engineering 100(3):183–221
32. Kundu A, Matthies H, Friswell M (2018) Probabilistic optimization of engineering system with prescribed target design in a reduced parameter space. Computer Methods in Applied Mechanics and Engineering 337:281–304
33. Luo Y, Niu Y, Li M, Kang Z (2017) A multi-material topology optimization approach for wrinkle-free design of cable-suspended membrane structures. Computational Mechanics 59:967–980, DOI https://doi.org/10.1007/s00466-017-1387-2
34. Maître OPL, Knio OM (2010) Spectral Methods for Uncertainty Quantification: With Applications to Computational Fluid Dynamics. Springer Netherlands
35. Michell MCE AGM (1904) Lviii. the limits of economy of material in frame-structures. The London, Edinburgh, and Dublin Philosophical Magazine and Journal of Science 8:589–597, DOI https://doi.org/10.1080/14786440409463229
36. Nanthakumar SS, Valizadeh N, Park HS, Rabczuk T (2015) Surface effects on shape and topology optimization of nanostructures. Computational Mechanics 56:97–112, DOI https://doi.org/10.1007/s00466-015-1159-9
37. Nguyen-Xuan H (2017) A polytree-based adaptive polygonal finite element method for topology optimization. International Journal for Numerical Methods in Engineering 110(10):972–1000, DOI 10.1002/nme.5448, URL https://onlinelibrary.wiley.com/doi/abs/10.1002/nme.5448, https://onlinelibrary.wiley.com/doi/pdf/10.1002/nme.5448
38. Park J, Sutradhar A, Shah JJ, Paulino GH (2018) Design of complex bone internal structure using topology optimization with perimeter control. Computers in Biology and Medicine pp –, DOI https://doi.org/10.1016/j.compbiomed.2018.01.001
39. Pereira A, Talischi C, Paulino GH, Menezes IFM, Carvalho MS (2016) Fluid flow topology optimization in polytop: stability and computational imple-

mentation. Structural and Multidisciplinary Optimization 54:1345–1364, DOI 10.1007/s00158-014-1182-z
40. Perrin G, Soize C, Duhamel D, Funfschilling C (2013) Karhunen–Loève expansion revisited for vector-valued random fields: Scaling, errors and optimal basis. Journal of Computational Physics 242:607–622, DOI https://doi.org/10.1016/j.jcp.2013.02.036
41. Pettersson MP, Iaccarino G, Nordström J (2015) Polynomial Chaos Methods for Hyperbolic Partial Differential Equations: Numerical Techniques for Fluid Dynamics Problems in the Presence of Uncertainties. Springer International Publishing
42. Putek P, Pulch R, Bartel A, ter Maten EJW, Günther M, Gawrylczyk KM (2016) Shape and topology optimization of a permanent-magnet machine under uncertainties. Journal of Mathematics in Industry 6:11, DOI https://doi.org/10.1186/s13362-016-0032-6
43. Qizhi Q, Kang Z, Wang Y (2014) A topology optimization method for geometrically nonlinear structures with meshless analysis and independent density field interpolation. Computational Mechanics 54:629–644, DOI https://doi.org/10.1007/s00466-014-1011-7
44. Richardson J, Filomeno Coelho R, Adriaenssens S (2016) A unified stochastic framework for robust topology optimization of continuum and truss-like structures. Engineering Optimization 48:334–350, DOI http://dx.doi.org/10.1080/0305215X.2015.1011152
45. Romero JS, Silva ECN (2014) A topology optimization approach applied to laminar flow machine rotor design. Computer Methods in Applied Mechanics and Engineering 279:268–300, DOI https://doi.org/10.1016/j.cma.2014.06.029
46. Rubinstein RY, Kroese DP (2016) Simulation and the Monte Carlo Method, 3rd edn. Wiley
47. Shin S, Samanlioglu F, Cho BR, Wiecek MM (2011) Computing trade-offs in robust design: Perspectives of the mean squared error. Computers & Industrial Engineering 60:248 –255, DOI https://doi.org/10.1016/j.cie.2010.11.006
48. Sigmund O, Petersson J (1998) Numerical instabilities in topology optimization: A survey on procedures dealing with checkerboards, mesh-dependencies and local minima. Structural Optimization 16:68–75, DOI https://doi.org/10.1007/BF01214002
49. Soize C (2013) Stochastic modeling of uncertainties in computational structural dynamics - recent theoretical advances. Journal of Sound and Vibration 332:2379—2395, DOI https://doi.org/10.1016/j.jsv.2011.10.010
50. Soize C (2015) Polynomial chaos expansion of a multimodal random vector. SIAM/ASA Journal on Uncertainty Quantification 3:34–60, DOI https://doi.org/10.1137/140968495
51. Soize C (2017) Uncertainty Quantification: An Accelerated Course with Advanced Applications in Computational Engineering. Springer International Publishing
52. Soize C, Desceliers C (2010) Computational aspects for constructing realizations of polynomial chaos in high dimension. SIAM Journal on Scientific Computing 32:2820–2831, DOI https://doi.org/10.1137/100787830
53. Soize C, Ghanem R (2004) Physical systems with random uncertainties: Chaos representations with arbitrary probability measure. SIAM Journal on Scientific Computing 26:395–410, DOI https://doi.org/10.1137/S1064827503424505

54. Soize C, Ghanem R (2017) Polynomial chaos representation of databases on manifolds. Journal of Computational Physics 335:201–221, DOI https://doi.org/10.1016/j.jcp.2017.01.031
55. Spanos PD, Ghanem R (1989) Stochastic finite element expansion for random media. Journal of Engineering Mechanics 115:1035–1053, DOI https://doi.org/10.1061/(ASCE)0733-9399(1989)115:5(1035)
56. Stefanou G (2009) The stochastic finite element method: Past, present and future. Computer Methods in Applied Mechanics and Engineering 198:1031–1051, DOI https://doi.org/10.1016/j.cma.2008.11.007
57. Svanberg K (1987) The method of moving asymptotes—a new method for structural optimization. International Journal for Numerical Methods in Engineering 24:359–373, DOI http://dx.doi.org/10.1002/nme.1620240207
58. Talischi C, Paulino GH, Pereira A, Menezes IFM (2010) Polygonal finite elements for topology optimization: A unifying paradigm. International Journal for Numerical Methods in Engineering 82:671–698, DOI http://dx.doi.org/10.1002/nme.2763
59. Talischi C, Paulino GH, Pereira A, Menezes IFM (2012) PolyTop: a Matlab implementation of a general topology optimization framework using unstructured polygonal finite element meshes. Structural and Multidisciplinary Optimization 45:329–357, DOI https://doi.org/10.1007/s00158-011-0696-x
60. Tootkaboni M, Asadpoure A, Guest JK (2012) Topology optimization of continuum structures under uncertainty – A polynomial chaos approach. Computer Methods in Applied Mechanics and Engineering 201–204:263–275, DOI https://doi.org/10.1016/j.cma.2011.09.009
61. Wu J, Gao J, Luo Z, Brown T (2016) Robust topology optimization for structures under interval uncertainty. Advances in Engineering Software 99:36 – 48, DOI https://doi.org/10.1016/j.advengsoft.2016.05.002, URL `http://www.sciencedirect.com/science/article/pii/S0965997816300874`
62. Xia L, Da D, Yvonnet J (2018) Topology optimization for maximizing the fracture resistance of quasi-brittle composites. Computer Methods in Applied Mechanics and Engineering 332:234–254, DOI https://doi.org/10.1016/j.cma.2017.12.021
63. Xiu D (2010) Numerical Methods for Stochastic Computations: A Spectral Method Approach. Princeton University Press
64. Xiu D, Karniadakis GE (2002) The Wiener-Askey Polynomial Chaos for stochastic differential equations. SIAM Journal on Scientific Computing 24:619–644, DOI https://doi.org/10.1137/S1064827501387826
65. Zhang W, Kang Z (2017) Robust shape and topology optimization considering geometric uncertainties with stochastic level set perturbation. International Journal for Numerical Methods in Engineering 110:31–56, DOI http://dx.doi.org/10.1002/nme.5344
66. Zhang XS, de Sturler E, Paulino GH (2017) Stochastic sampling for deterministic structural topology optimization with many load cases: Density-based and ground structure approaches. Computer Methods in Applied Mechanics and Engineering 325:463–487, DOI https://doi.org/10.1016/j.cma.2017.06.035
67. Zhang XS, Paulino GH, Ramos AS (2018) Multi-material topology optimization with multiple volume constraints: a general approach applied to ground structures with material nonlinearity. Structural and Multidisciplinary Optimization 57:161–182, DOI https://doi.org/10.1007/s00158-017-1768-3

68. Zhao J, Wang C (2014) Robust structural topology optimization under random field loading uncertainty. Structural and Multidisciplinary Optimization 50:517–522, DOI https://doi.org/10.1007/s00158-014-1119-6